Optics and Laser Technology 121 (2020) 105813

Contents lists available at ScienceDirect

Optics and Laser Technology

journal homepage: www.elsevier.com/locate/optlastec

Full length article

Resonantly pumped mid-infrared Ho:YAG/$BaWO_4$ intracavity Raman laser at 2640 nm

Xinlu Zhang[a,b,*], Kaibo Ni[a], Jinjer Huang[a], Guangzong Dong[a], Guoxing Li[c]

[a] School of Physics Science and Technology, Tiangong University, Tianjin 300387, China
[b] Key Laboratory of In-Fiber Integrated Optics (Ministry of Education) and College of Science, Harbin Engineering University, Harbin 150001, China
[c] Heilongjiang Electric Power Research Institute, Harbin 150030, China

HIGHLIGHTS

- First demonstration of a Ho:YAG/$BaWO_4$ intracavity Raman laser at 2640 nm.
- Highest peak power of 14.4 kW is obtained at the repetition frequency of 1 kHz.
- Maximum output power of 473 mW is achieved at the repetition frequency of 5 kHz.

ARTICLE INFO

Keywords:
Solid state laser
Actively Q-switched
Ho:YAG
Mid-infrared

ABSTRACT

We report on a mid-infrared 2640 nm intracavity Raman laser based on $BaWO_4$ Raman conversion in a resonantly pumped actively Q-switched Ho:YAG laser. At the pulse repetition frequency of 1 kHz, the threshold pump power is as low as 2.1 W at 1.91 μm. Increasing the incident pump power to 3.6 W, the pulse energy and the pulse width are 105 μJ and 7.32 ns respectively, which corresponds to a peak power as high as 14.4 kW. When the pulse repetition frequency is increased to 5 kHz, the maximum average output power of 473 mW is achieved under a 9.8 W incident pump power. The mid-infrared pulse laser has potential applications in chemical sensing, environmental monitoring, and laser medicine.

1. Introduction

Stimulated Raman scattering (SRS) is a very important and effective nonlinear frequency conversion method. Solid state Raman lasers based on the SRS effect can generate new laser wavelengths, which are usually difficult to obtain in the direct laser oscillation [1–3]. It is widely known that both the wavelength of fundamental laser and the Raman frequency shift of Raman crystal decide the output wavelength of a Raman laser [4]. With the development of high quality Raman crystals, solid state Raman lasers have attracted increasing attention [5–11]. Among these known Raman crystals, $BaWO_4$ is an excellent candidate which has been widely investigated, due to high Raman gain coefficient, high optical damage threshold, and good mechanical and thermal properties [12,13]. In the past few years, the research of solid state Raman laser based on $BaWO_4$ crystal was focused on the near-infrared spectral region [14–22]. The mid-infrared Raman lasers based on $BaWO_4$ crystal were reported very little. The 2–3 μm mid-infrared lasers have very important applications in laser medicine, chemical sensing, and environmental monitoring [23,24]. So, it is very meaningful to investigate the 2–3 μm mid-infrared lasers. However, it is a challenge to realize efficient mid-infrared Raman lasers, because the Raman gain coefficient of Raman crystal is almost inversely proportional to the wavelength of pump laser [1].

Pumping the $BaWO_4$ Raman crystal with pulse lasers, SRS in mid-infrared spectral range 2.31–2.75–3.7 μm was observed, moreover the external-cavity $BaWO_4$ Raman laser at 2602 nm was also realized [24,25]. The intracavity Raman laser has a relatively low threshold pump power and the effect of beam clean-up, comparing with the external-cavity Raman laser [8]. To date, the intracavity solid state Raman lasers have been widely investigated in the wavelength range from 1.07 to 1.7 μm, however the 2–3 μm mid-infrared intracavity solid Raman lasers have seldom been reported. Batay et al. first observed the weak 2365 nm self-Raman spectrum in a 1950 nm passively Q-switched Tm:$KY(WO_4)_2$ laser in 2002 [26]. Our research group demonstrated the mid-infrared 2360 nm $BaWO_4$ and 2418 nm YVO_4 Raman lasers intracavity-pumped by a diode-end-pumped actively Q-switched Tm:YAP laser [27,28]. However, the Tm-doped materials were generally used in the low output energy lasers due to the small emission cross section

* Corresponding author.
E-mail address: zhangxinlu@tjpu.edu.cn (X. Zhang).

https://doi.org/10.1016/j.optlastec.2019.105813
Received 15 April 2019; Received in revised form 3 September 2019; Accepted 4 September 2019
Available online 16 September 2019
0030-3992/

[29]. The diode-end-pumped actively Q-switched Tm,Ho:$GdVO_4$/$BaWO_4$ intracavity Raman laser at 2553 nm was also reported [30,31]. While the Tm-Ho codoped crystals needed cooling with liquid nitrogen to enhance the output efficiency [30–32]. At present, Ho-doped solid state lasers are particularly attractive for Q-switched operation near room temperature, because of large emission cross section and long upper level lifetime. Moreover, resonant pumping of the Ho single doping materials has many advantages, such as low quantum defect, low upconversion losses, and low sensitivity of temperature [33–35].

In this paper, the intracavity Ho:YAG/$BaWO_4$ Raman laser at 2640 nm is first demonstrated, which is resonantly pumped by a 1908 nm continuous wave Tm:YLF laser. At the incident pump power of 9.8 W and the pulse repetition frequency (PRF) of 5 kHz, the Raman laser produces an average output power of 473 mW at 2640 nm. At the PRF of 1 kHz, the threshold pump power is only 2.1 W and the pulse peak power is as high as 14.4 kW. To the best of our knowledge, this is the first resonantly pumped intracavity $BaWO_4$ Raman laser in the mid-infrared spectral region.

2. Experimental setup

The schematic diagram of experimental setup for the resonantly end-pumped actively Q-switched Ho:YAG/$BaWO_4$ intracavity Raman laser is shown in Fig. 1. The pump source is a home-built continuous wave Tm:YLF laser, which has a maximum output power of 10 W. The output wavelength of the Tm:YLF laser is tuned to 1908 nm by carefully adjusting the tilting angle of an intracavity 100 μm thick etalon. Ho:YAG crystal has a suitable absorption peak at 1908 nm. The gain medium used to generate the fundamental laser is a 1 at.% doped Ho:YAG crystal with dimensions of 4 mm × 4 mm × 30 mm. Both end faces of the Ho:YAG crystal are anti-reflection coated at 1900–2150 nm. The pump light is focused into the Ho:YAG crystal by a spherical lens with a focal length of 75 mm, and the spherical lens is anti-reflection coated at 1908 nm. The diameter of the focused pump laser is approximately 400 μm in the Ho:YAG crystal. The a-cut $BaWO_4$ crystal with dimensions of 4 mm × 4 mm × 20 mm is chosen as the Raman active medium, and it is anti-reflection coated in the range of 1800–2700 nm (R < 3%). Both the Ho:YAG and $BaWO_4$ crystals are wrapped with indium foil and mounted on water-cooled copper heat sinks, which are kept at a temperature of 289 K by two thermoelectric coolers, respectively. A 36 mm long fused silica Brewster-cut acousto-optic Q-switch (The 26th Electronics Institute, Chinese Ministry of Information Industry) is anti-reflection coated at 2 μm on both faces, and driven with a radio frequency power of 50 W at the ultrasonic frequency of 40.68 MHz.

A coupled cavity with a linear configuration is adopted for the Ho:YAG/$BaWO_4$ Raman laser. The fundamental resonator is composed of the mirrors M1 and M3, and the length of the cavity is 170 mm. Mirrors M2 and M3 compose the Raman resonator, whose length is 40 mm. The flat input mirror M1 has been coated for high transmittance (T > 99.5%) at 1908 nm and high reflection (R > 99.8%) at 2122 nm. The mirror M3 with a curvature radius of 200 mm is coated for high reflection at 2122 nm (R > 99.5%) and partial reflection at 2640 nm (R = 90%), and it is also utilized as the output coupler of Raman laser. One surface of the flat intracavity mirror M2 is anti-reflection coated at 2122 nm (R < 1%), and the other surface is coated for anti-reflection (R < 1%) at 2122 nm and high reflection (R > 99.8%) at 2640 nm. A 45° flat dichroic mirror M4 is used to separate the residual fundamental and Raman laser, which has high transmittance at 2640 nm and high reflection at 2122 nm respectively. The output spectrum of the Raman laser is monitored by a 300 mm monochromator (Omni-λ 300, Zolix) and an InGaAs detector. The average output power is measured by a power meter (PM30, Coherent Inc.). The pulse energy is measured by an energy meter (J-25MT-10 kHz, Coherent Inc.). The pulse temporal behaviors of the fundamental and Raman lasers are recorded by a 300 MHz bandwidth digital phosphor oscilloscope (TDS 3032B, Tektronix) with an infrared detector (PVM-10.6, VIGO). The spatial profile of Raman laser is measured by a beam analyzer (MicronViewer 7290A, Electrophysics).

3. Experimental results

The output performances of the resonantly pumped Ho:YAG/$BaWO_4$ intracavity Raman laser are investigated at different pump powers and PRFs. We first measure the output spectra of the Ho:YAG/$BaWO_4$ intracavity Raman laser. To measure the output spectra of the fundamental laser and the Raman laser simultaneously, the dichroic mirror M4 should be removed. The wavelengths of the fundamental and the first Stokes laser are 2122 nm and 2640 nm respectively, as shown in Fig. 2. It can be observed that the value of frequency shift between the fundamental and the first Stokes laser is approximately 925 cm^{-1}, which agrees very well with the optical vibration modes of tetrahedral WO_4^{-2}. In our experiment, only the first Stokes laser is observed, and no higher Stokes laser appears.

Fig. 3(a) plots the average output power of the 2640 nm Raman laser as a function of incident pump power for the PRFs of 1, 2, 3, 4, and 5 kHz. The threshold pump power of the Raman laser strongly depends on the PRF and decreases from 5.3 to 2.1 W when the PRF is changed from 5 to 1 kHz. The threshold pump power of the Raman laser decreases when reducing the PRF, however, the average output power shows severe saturation at a relatively low PRF because of the self-focusing-induced damage to the $BaWO_4$ Raman crystal [5,17]. At the PRF of 1 kHz, the average output power of Raman laser almost linearly increases with the pump power before the pump power is increased to 3.3 W. Then the average output power shows obvious saturation with the further increasing of pump power. When the PRF is increased to 5 kHz, a highest average output power of 473 mW is achieved at the incident pump power of 9.8 W, which corresponds to an optical conversion of 4.8% from Tm:YLF laser pump power to Raman output power. Fig. 3(b) plots the single pulse energy as a function of incident pump power for the PRFs from 1 to 5 kHz. It can be found from Fig. 3(b) that the single pulse energy has a maximum value of 105 μJ at the PRF of 1 kHz and the pump power of 3.6 W. The pulse width of Raman laser as a function of incident pump power is also measured at the PRFs from 1 to 5 kHz, as shown in Fig. 3(c). The pulse width increases with the PRF for the same pump power, and the narrowest pulse width of 7.32 ns is achieved at the PRF of 1 kHz. According to the relation of pulse energy and pulse width, the pulse peak power of Raman laser as a function

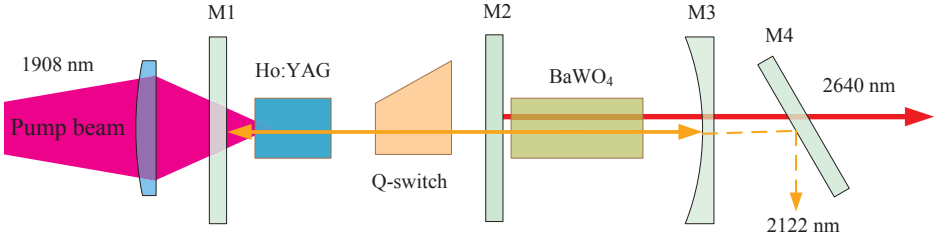

Fig. 1. The experimental setup of the resonantly pumped actively Q-switched Ho:YAG/$BaWO_4$ mid-infrared intracavity Raman laser.

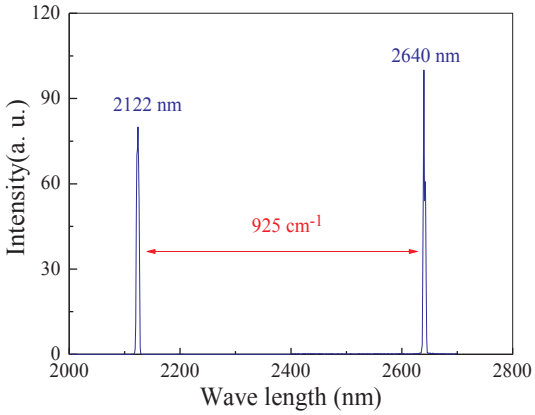

Fig. 2. Optical spectra of the fundamental and Raman laser.

of incident pump power is given in Fig. 3(d). The peak power of Raman laser increases with the increase of incident pump power and decreases with the increase of PRF, and the highest pulse peak power of 14.4 kW is obtained at the PRF of 1 kHz and the pump power of 3.6 W as shown in Fig. 3(d).

At the PRF of 1 kHz and the pump power of 3.6 W, the typical pulse shape and the train of output pulses for the Raman laser are shown in Fig. 4. The pulse widths of the fundamental laser and the Raman laser are approximately 54 and 7.32 ns respectively, as given in Fig. 4(a). The pulse width of the Raman laser is much narrower than that of the fundamental laser, which indicates that the SRS process indeed plays a role in pulse compression [5].

The insets in Fig. 5 show the beam profiles of Raman laser at the average output power of 473 mW and the PRF of 5 kHz. The spatial profile of the Raman laser is close to a fundamental transverse electromagnetic (TEM_{00}) mode. For evaluating the beam quality of Raman laser, the beam radius along the beam propagation direction is

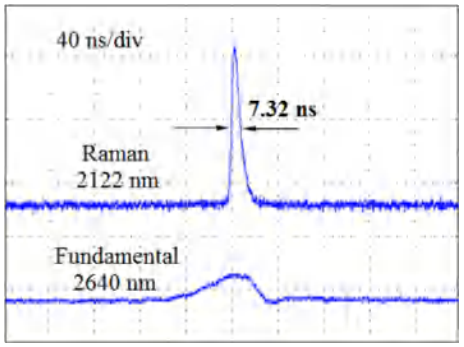

Fig. 4. Oscilloscope traces of the single fundamental pulse and single Raman pulse at the PRF of 1 kHz and the pump power of 3.6 W.

measured through a 100 mm focal length lens. The beam radii are measured at different positions by the traveling knife-edge method, as shown in Fig. 5. The fitted beam quality factor M^2 is equal to 1.2. The spatial profiles of the Raman laser are also measured at other pump powers and PRFs, and always show a good single transverse mode.

4. Conclusion

In summary, the resonantly pumped actively Q-switched Ho:YAG/$BaWO_4$ intracavity Raman laser at 2640 nm has been demonstrated. A compact coupled cavity configuration is adopted to investigate the output performances of the Ho:YAG/$BaWO_4$ Raman laser, and stable 2640 nm Raman laser is achieved. At the PRF of 5 kHz and the incident pump power of 9.8 W at 1908 nm, the maximum average output power of the 2640 nm Raman laser is 473 mW. At the PRF of 1 kHz, the $BaWO_4$ Raman laser has a low threshold pump power of 2.1 W. When the pump power is increased to 3.6 W, the maximum pulse energy is 105 μJ, the shortest pulse width is 7.32 ns, and the corresponding pulse peak power

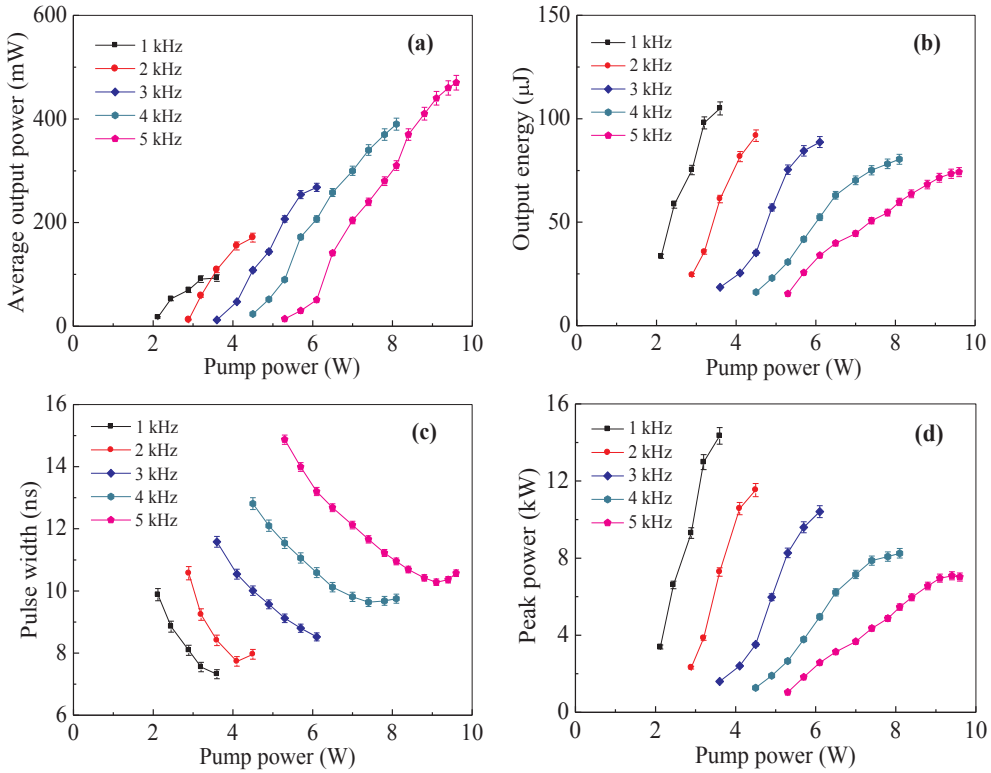

Fig. 3. (a) Average output power, (b) pulse energy, (c) pulse width, and (d) peak power at the Stokes wavelength of 2640 nm as the functions of incident pump power at different PRFs from 1 to 5 kHz.

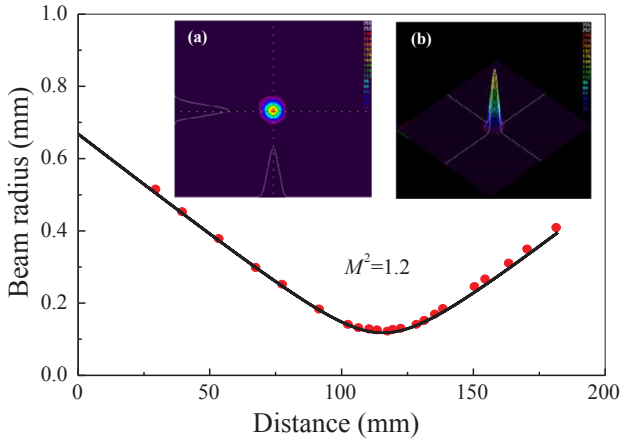

Fig. 5. Beam radius of the Ho:YAG/$BaWO_4$ Raman laser as a function of the distance from the 100 mm focusing lens at the maximum output power of 473 mW for the 5 kHz PRF. Insets (a) and (b) show the two and three dimensional beam profiles respectively.

is 14.4 kW. The mid-infrared pulse laser with high peak power has potential applications in high resolution molecular spectroscopy and remote sensing.

Acknowledgment

This research is supported by the National Natural Science Foundation of China (61775166, 61275138), the Nature Science Foundation of Tianjin (19JCZDJC32600), the 111 Project to the Harbin Engineering University (B13015), and the Program for Innovatative Research Team in University of Tianjin (TD13-5035). The authors thank Professor Huaijin Zhang (Key Laboratory of Crystal Material of Shandong University) for providing the $BaWO_4$ sample.

Appendix A. Supplementary data

Supplementary data to this article can be found online at https://doi.org/10.1016/j.optlastec.2019.105813.

References

[1] H.M. Pask, Progr. Quantum Electron. 27 (1) (2003) 3–56.
[2] J.A. Piper, H.M. Pask, IEEE J. Sel. Top. Quantum Electron. 13 (3) (2007) 692–704.
[3] P. Cerny, H. Jelinkova, P.G. Zverev, T.T. Basiev, Progr. Quantum Electron. 28 (2) (2004) 113–143.
[4] V.G. Savitski, S. Reilly, A.J. Kemp, IEEE J. Quantum Electron. 49 (2) (2013) 218–223.
[5] Y.F. Chen, K.W. Su, H.J. Zhang, J.Y. Wang, M.H. Jiang, Opt. Lett. 30 (24) (2005) 3335–3337.
[6] T.T. Basiev, M.N. Basieva, A.V. Gavrilov, M.N. Ershkov, L.I. Ivleva, V.V. Osiko, S.N. Smetanin, A.V. Fedin, Quantum Electron. 40 (8) (2010) 710–715.
[7] R.J. Williams, D.J. Spence, O. Lux, R.P. Mildren, Opt. Express 25 (2) (2017) 749–757.
[8] J.T. Murray, W.L. Austin, R.C. Powell, Opt. Mater. 11 (4) (1999) 353–371.
[9] X. Ding, C. Fan, Q. Sheng, B. Li, X.Y. Yu, G.Z. Zhang, B. Sun, L. Wu, H.Y. Zhang, J. Liu, P.B. Jiang, W. Zhang, C. Zhao, J.Q. Yao, Opt. Express 22 (23) (2014) 29111–29116.
[10] J. Liu, X. Ding, P.B. Jiang, Q. Sheng, X.Y. Yu, B. Sun, R. Shi, J.B. Wang, Y.T. Bai, L. Zhao, G.Z. Zhang, L. Wu, J.Q. Yao, Opt. Express 26 (8) (2018) 10171–10178.
[11] X.L. Wang, J. Dong, X.J. Wang, J. Xu, K. Ueda, A.A. Kaminskii, Opt. Lett. 41 (15) (2016) 3559–3562.
[12] G.M. Bonner, H.M. Pask, A.J. Lee, A.J. Kemp, J.Y. Wang, H.J. Zhang, T. Omatsu, Opt. Express 20 (9) (2012) 9810–9818.
[13] L. Fan, Y.X. Fan, Y.Q. Li, H.J. Zhang, Q. Wang, J. Wang, H.T. Wang, Opt. Lett. 34 (11) (2009) 1687–1689.
[14] W.J. Sun, Q.P. Wang, Z.J. Liu, X.Y. Zhang, G.T. Wang, F. Bai, W.X. Lan, X.B. Wan, H.J. Zhang, Laser Phys. Lett. 8 (7) (2011) 512–515.
[15] M. Frank, S.N. Smetanin, M. Jelínek, D. Vyhlídal, L.I. Ivleva, P.G. Zverev, V. Kubeček, Opt. Lett. 43 (11) (2018) 2527–2530.
[16] H.N. Zhang, X.H. Chen, Q.P. Wang, P. Li, Laser Phys. Lett. 11 (10) (2014) 105806.
[17] H.N. Zhang, X.H. Chen, Q.P. Wang, X.Y. Zhang, J. Chang, L. Gao, H.B. Shen, Z.H. Cong, Z.J. Liu, X.T. Tao, P. Li, Opt. Lett. 39 (9) (2014) 2649–2651.
[18] X.H. Chen, P. Li, X.Y. Zhang, Q.P. Wang, Z.J. Liu, Z.H. Cong, L. Li, H.J. Zhang, Laser Phys. 21 (12) (2011) 2040–2044.
[19] H.B. Shen, Q.P. Wang, P. Li, G.P. Li, X.Y. Zhang, Z.J. Liu, X.H. Chen, Z.H. Cong, L. Guo, X.T. Tao, H.J. Zhang, J.X. Fang, Opt. Commun. 306 (2013) 165–169.
[20] H.B. Shen, Q.P. Wang, X.Y. Zhang, X.H. Chen, Z.H. Cong, Z.G. Wu, F. Bai, W.X. Lan, L. Gao, Opt. Express 20 (16) (2012) 17823–17832.
[21] H.B. Shen, Q.P. Wang, X.Y. Zhang, X.H. Chen, F. Bai, Z.J. Liu, L. Gao, Z.H. Cong, Z.G. Wu, W.T. Wang, Y.G. Zhang, W.X. Lan, C. Wang, Opt. Lett. 37 (21) (2012) 4519–4521.
[22] Y.C. Zhang, L. Fan, C.F. Wei, X.M. Gu, S.X. Ren, Acta Phys. Sin. 67 (2) (2018) 024206.
[23] Q. Gaimard, M. Triki, T. Nguyen-Ba, L. Cerutti, G. Boissier, R. Teissier, A. Baranov, Y. Rouillard, A. Vicet, Opt. Express 23 (15) (2015) 19118–19128.
[24] T.T. Basiev, M.N. Basieva, M.E. Doroshenko, V.V. Fedorov, V.V. Osiko, S.B. Mirov, Laser Phys. Lett. 3 (1) (2006) 17–20.
[25] O. Kuzucu, Opt. Lett. 40 (21) (2015) 5078–5081.
[26] L.E. Batay, A.N. Kuzmin, A.S. Grabtchikov, V.A. Lisinetskii, V.A. Orlovich, A.A. Demidovich, A.N. Titov, V.V. Badikov, S.G. Sheina, V.L. Panyutin, M. Mond, S. Küch, Appl. Phys. Lett. 81 (16) (2002) 2926–2928.
[27] J.Q. Zhao, Y. Li, S. Zhang, L. Li, X.L. Zhang, Opt. Express 23 (8) (2015) 10075–10080.
[28] P. Cheng, J.Q. Zhao, F. Xu, X.F. Zhou, G.D. Wang, Appl. Phys. B 124 (1) (2018) 5.
[29] W. Cai, J. Liu, C. Li, H.T. Zhu, P.G. Ge, L.H. Zheng, L.B. Su, J. Xu, Opt. Commun. 334 (2015) 287–289.
[30] J.Q. Zhao, X.L. Zhang, X. Guo, X.J. Bao, L. Li, J.H. Cui, Opt. Lett. 38 (8) (2013) 1206–1208.
[31] X.L. Zhang, Y. Ding, Y. Qiao, G.X. Li, J.H. Cui, Opt. Commun. 355 (2015) 433–437.
[32] L.J. Li, X.N. Yang, L. Zhou, W.Q. Xie, Y.L. Wang, Y.J. Shen, Y.Q. Yang, W.L. Yang, W. Wang, Z.W. Lv, X.M. Duan, M.H. Chen, Photon. Res. 6 (6) (2018) 614–619.
[33] L. Wang, C.Q. Gao, M.W. Gao, Y. Li, F.Y. Yue, J. Zhang, D.Y. Tang, Opt. Express 22 (1) (2013) 254–261.
[34] J.H. Yuan, X.M. Duan, B.Q. Yao, J. Li, Z. Cui, Y.J. Shen, T.Y. Dai, Y.L. Ju, C.Y. Li, H.M. Kou, Y.B. Pan, Appl. Phys. B 119 (2) (2015) 381–385.
[35] J.W. Kim, J.I. Mackenzie, D. Parisi, S. Veronei, M. Tonelli, W.A. Clarkson, Opt. Lett. 35 (3) (2010) 420–422.